Modeling the Membrane Binding Mechanism of a Lipid Transport Protein Osh4 to Single Membranes

Sharmistha Karmakar[1] and Jeffery B. Klauda[1,2,*]
[1]Department of Chemical and Biomolecular Engineering
[2]Biophysics Graduate Program
University of Maryland, College Park, MD 20742, USA
*Corresponding Author: jbklauda@umd.edu

Abstract:

All atom molecular dynamics simulations are utilized to unravel the binding mechanism of yeast oxysterol binding protein (Osh4) to model membranes with varying anionic lipid concentration using all-atom (AA) and the highly mobile membrane mimetic (HMMM) representations. For certain protein-lipid interactions, an improved force field description is used (CUFIX) to accurately describe lipid-protein electrostatic interactions. Our detailed computational studies have identified a single, β-crease orientated, membrane bound conformation of Osh4 for all anionic membranes. The penetration of the PHE-239 residue below the membrane phosphate plane is the characteristic signature of the membrane-bound state of Osh4. As the phenylalanine loop anchors itself deeply in the membrane; the other regions of the Osh4, namely, ALPS motif, ß6- ß7 loop, ß14- ß15 loop and ß16- ß17 loop, maximize their contact with the membrane. Furthermore, loose lipid packing and higher mobility of HMMM enables stronger association of ALPS motif with the membrane lipids through its hydrophobic surface and after the HMMM is converted to AA and equilibrated the binding is 2-3 times stronger compared to simulations started with the AA representation yielding the major importance of the ALPS motif to binding. Quantitative estimation of binding energy revealed that the phenylalanine loop plays a crucial role in stable membrane attachment of Osh4 and contributes significantly toward overall binding process. The CUFIX parameters provide a more balanced picture of hydrophobic and electrostatic interactions between the protein and the membrane which differs from our past work that showed salt bridges alone stabilized Osh4-membrane contact. Our study provides a comprehensive picture of the binding mechanism of Osh4 with model single membranes and thus, understanding of the initial interactions is important for elucidating the biological function of this protein to shuttle lipids between organelles.

Statement of Significance:

The membrane composition of various cellular organelles displays wide heterogeneity and the functions of membrane proteins are strongly governed by these lipid microenvironments. Lipid transfer proteins namely, oxysterol-binding protein-related proteins regulate the trafficking of lipids across cellular compartments via non-vesicular transport mechanism and maintain the widespread diversity of cellular membranes. The present study explores the membrane binding dynamics of yeast oxysterol binding protein (Osh4) to model membranes with varying anionic lipid concentration using microsecond long all-atom molecular dynamics simulations. Our detailed computational studies utilizing a modified protein force field (CHARMM36m) and more accurate description for lipid-protein electrostatic interactions (CUFIX) have identified a single, β-crease orientated, membrane bound conformation of Osh4 for all anionic membranes.

Introduction:

Peripheral membrane proteins are a class of membrane proteins that bind transiently to the surface of the cellular membrane predominantly via electrostatic or hydrophobic interactions. They possess variety of conserved membrane-targeting domains such as pleckstrin homology (PH), protein kinase C conserved 1, protein kinase C conserved 2, epsin amino-terminal homology, Phox, Bin/Amphiphysin/Rvs (BAR), and tubby domains, which facilitate the membrane recognition process with their unique structural features.(1-3) The membrane association process often requires the presence of specific lipid microenvironment or curvature at the binding surface. Recent studies have identified that the presence of signaling lipids, i.e., PIPs, act as a guiding factor for the recruitment of PH domains for a variety of membrane proteins, e.g., G protein-coupled receptor kinases, phospholipase C-delta 1 and protein kinase AKT1.(4-6) Hence, the cellular functions of peripheral proteins are regulated by the local lipid environment and their ability to bind to a specific membrane in a reversible manner. Thus, maintaining a distinct lipid composition for a particular cellular compartment is crucial for accurate functioning of the organelle.

The lipid landscape of different organelles exhibits remarkable structural and functional diversity. For example, sterol, another fundamental membrane component, is present in highest concentration (~40%) at the plasma membrane (PM), while its level is substantially low (~ 5%) at its production site i.e., the endoplasmic reticulum (ER).(7,8) As, a majority of lipids are synthesized at the ER, they must be effectively transported to other organelles in order to maintain such lipid diversity.(9) There are two dedicated pathways for intracellular lipid trafficking, vesicular and non-vesicular transport mechanism, among which the non-vesicular lipid transport has gained renewed attention in recent years. The non-vesicular transport mechanism is particularly important for those organelles that do not participate in secretory pathways (e. g, mitochondria).(10,11) Lipid transfer proteins (LTPs) (12) are the key player for lipid trafficking through this pathway. Although the exact mechanism of operation for such LTPs is still unknown, several *in vivo* and *in vitro* experimental studies have identified two major pathways.(13,14) While, one theory suggests that LTPs extract lipids from a donor membrane and shield the lipid in its hydrophobic cavity from exterior and then transfer it to the acceptor membrane by diffusing

through cytoplasm. Another prevailing theory states that LTP operates at membrane contact sites (MCSs) where two membranes are closely apposed (within 30 nm) and in this scenario the LTP establishes contact with both the membranes simultaneously and shuttles the lipid across two membranes through a hydrophobic channel.(14,15) The mode of action by which LTP targets a specific membrane and how it mediates lipid transport at MCS and what are other factors (for example, physiological conditions or membrane composition and curvature or tethering proteins) that facilitate the formation and stabilization of such highly dynamic contact sites between two organelles is not well understood.

The Oxysterol binding protein (OSBP) family, comprising of OSBP-related proteins (ORPs) in mammals and its homologous version known as Osh in yeast, was originally identified as a sterol binding protein. They are cytosolic proteins that are conserved from yeast to higher eukaryotes. All possess a common structural domain known as OSBP-related domain (ORDs), that facilitates the binding of oxysterol derivatives.(16-18) The physiological function of OSBPs is widespread ranging from sterol homeostasis to signal transduction.(16,18,19) Among seven yeast ORPs, Osh4p is the most abundantly expressed Osh protein that consists of solely the ORD domain and due to its structural simplicity, it is the best studied example till date.(20) In 2005, *Im et al.(21)* first reported the crystal structure of Osh4p protein complexed with several sterol derivatives and they identified Osh4p (Figure 1) as a β-barrel protein with 19 antiparallel β-sheet strands that form the hydrophobic core facilitating sterol capture. Additionally, there is an amphipathic α-helix positioned near mouth of the protein which acts as a physical barrier for the sterol from exterior aqueous environment.(21) The cellular function of yeast Osh4 proteins in intracellular sterol trafficking is still not well understood. *In vitro* experimental studies by Raychaudhuri et al. have demonstrated that Osh4p can transport sterol between liposomes and its transfer efficiency is greatly enhanced by the presence of anionic lipids (e. g, PS and PIPs) at the target membrane.(22) Moreover, it was also proposed that Osh4p acts as a sterol/PI(4)P exchanger where it acquires the sterol from donor membrane (ER) and exchanges it for a PI(4)P at acceptor membrane (trans-Golgi) and then carries the PI(4)P back to the donor membrane completing the exchange cycle.(23,24) In addition, the regulatory role of Osh4 through coupling with Sec14p (a protein of yeast that controls the PI4P levels at ER, Golgi, and PM) in post-Golgi vesicular trafficking was also established.(25,26) Thus, the exact physiological function of Osh4 inside cell is still

ambiguous, whether it acts as sterol transporter or regulator of MCS formation or lipid sensor that modulates the lipid metabolism, signaling and membrane composition need to be discovered.

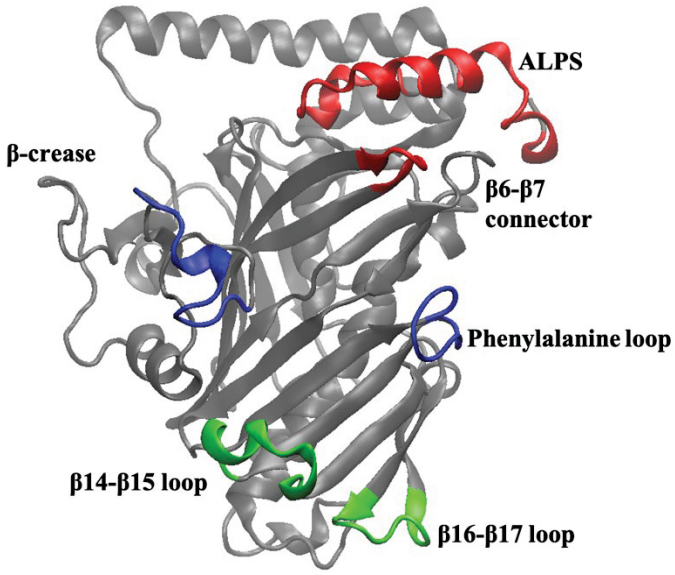

Figure 1. Structure of yeast Osh4 (obtained from PDB ID: IZHZ(21)). The membrane targeting domains are highlighted in color. The ALPS motif (residues 1 to 29) and ß6-ß7 connector (residues 172 to 177) are shown in red; ß14-ß15 loop (residues 253 to 264) and ß16-ß17 loop (residues 279 to 287) are shown in green and phenylalanine loop (residues 236 to 244) and ß-crease (residues 402 to 413) regions are highlighted in blue.

The membrane association of Osh4 is the primary step for all proposed cellular functions of this protein. Previous experimental and computational studies have suggested that Osh4 possesses multiple membrane binding surfaces, however, their explicit function in membrane recognition and binding process has not been resolved specifically.(23) In this study, using a modified protein force field (CHARMM36m)(27-29) and more accurate description for lipid-protein electrostatic interactions (CUFIX)(30), we have elucidated how the binding mechanism of Osh4 is affected by these new force field parameters using microsecond long all-atom molecular dynamics simulations. Additionally, as the binding conformation of peripheral membrane protein is strongly governed by the physical properties of the membrane, we have investigated the effect of lipid packing on the membrane binding mechanism of Osh4 utilizing the highly mobile membrane mimetic (HMMM)(31) model. Since, higher lipid mobility in HMMM accelerates the binding timescale for peripheral proteins by at least two orders of magnitude, we are able to unravel more binding details without compromising the atomistics details.

Methods:

Molecular dynamics (MD) simulation was utilized to study the interaction of a yeast oxysterol binding protein, Osh4, with model membranes. We have chosen three membrane compositions, i.e., acceptor, acceptor-PIP and donor membrane where the naming convention for each system has been kept in compliance with previous experimental and computational studies (23,32). The donor membrane is composed of 1,2-dioleoyl-sn-glycero-3-phosphocholine (DOPC), 1,2-dioleoyl-sn-glycero-3-phosphoethanolamine (DOPE), 1-palmitoyl-2-oleoyl-sn-glycero-3-phosphoethanolamine (POPE), 1-palmitoyl-2-oleoyl-sn-glycero-3-phospho-L-serine (POPS), 1-palmitoyl-2-oleoyl-inositol-(4,5)-bisphosphate [$PI(4,5)P_2$] and ergosterol (ERG) lipids, while the acceptor-PIP membrane possess DOPC, POPE and $PI(4,5)P_2$ lipids and the acceptor membrane have only DOPC and POPE lipids. The exact compositions of each membrane can be found in Table S1. The composition of model membranes differs in the percentage of anionic lipids with the donor membrane having the highest concentration of (~10%) anionic lipids followed by acceptor-PIP (~ 1%) and acceptor membrane (no anionic lipids). We have constructed the model membranes with 298 (for acceptor and acceptor-PIP) and 300 (for donor) lipid molecules respectively, which is divided equally among two leaflets. The protein structure was obtained from PDBID: 1zhz (21) The computational study was divided into two sets, one with highly mobile membrane mimetic (HMMM) model and other with all-atom (AA) full-tail description of lipid molecules.

The AA and HMMM models were built using *Membrane Builder* and *HMMM Builder* feature of CHARMM-GUI.(33-36) HMMM possesses lipid molecules which are truncated acyl chains at C6 position with original lipid head group and the hydrophobic membrane core is replaced by 1,1-dichloroethane (DCLE) molecules.(35) HMMM has been shown to increase the lipid diffusion by one or two orders of magnitude, thus, accelerates the association of protein with the membrane. The lipid area scaling factor was chosen to be 1.2.(31,37) The protein was placed approximately 5 to 10 Å away from the membrane surface and its orientation is modeled using rotation feature of CHARMM-GUI.(38) The protein was placed in three different orientations (mouth, crease and

distal) to sample feasible conformation of the protein and each membrane system was built accordingly. NTER and CTER patches were used to model the terminal group of the protein. Each system was solvated using minimum of 22.5 Å water layers on top and bottom of the system and TIP3P model(39) was used to model the water molecules. Finally, potassium ions and chloride ions were added to neutralize the system. All simulations were carried out using all-atom CHARMM36 (C36) force field for lipids(27,40) and C36m parameters for the protein(28,29) along with the CUFIX(30) parameter set that describes the protein-membrane electrostatic interaction more accurately. The new CUFIX parameter refines the non-bonded interactions between amine group of positively-charged amino acids and negatively-charged carboxylate and phosphate groups of lipids in such a way that eliminates unphysical attraction between protein and membrane resulting more realistic dynamics of the studied systems.

Each of the systems was initially equilibrated following standard six step CHARMM-GUI protocol for 225 ps.(41,42) Next, final production simulation was carried out with the last frame of the equilibrated system with a time step of 2 fs. The constant molecule number, pressure, and temperature (NPT) ensemble with temperature of 310 K and pressure of 1 bar, was employed for AA membrane systems while NPAT ensemble (where A represents constant lateral surface area of membrane) was used for HMMM. All the MD simulations were performed using NAMD software package.(43,44) Periodic boundary condition was employed for all the systems. The hydrogen atoms are constrained using SHAKE algorithm.(45) Langevin dynamics was used to keep the temperature constant at 310 K with a damping coefficient of 1 ps^{-1} and the pressure was maintained using the Nosé−Hoover Langevin piston.(46-48) Non-bonded interactions were computed with a distance cutoff of 12 Å with a force-switching function applied over 10 to 12 Å.(49) The long-range electrostatics is modeled using particle mesh Ewald method with a grid density of >1 Å.(50) The production runs for all-atom systems were run for 1000 ns while for HMMM the simulations were carried out for 300 ns or until binding is achieved (whichever is earlier). Once membrane-bound conformation was reached, HMMM model was converted to full-length representation following additional 150 ns simulation run using NPT ensemble. Simulation snapshots were generated using VMD software.(51) Analysis, e.g., minimum distance profile, protein-membrane interaction energy, frequency of contact, relative Z position and electron density profile were performed in CHARMM software(42). While the heavy-

atom contact count and H-bond analysis were carried out in VMD using in-house Tcl scripts. Most of the analysis were performed at the membrane bound state of the protein, except the protein-membrane minimum distance profile calculation which was carried out for overall simulation time.

Results:

To unravel the membrane binding dynamics of Osh4, we have modeled three different lipid compositions in accordance with a previous experimental study where the percentage of anionic lipids varies from 0 to 10%.(22) According to previous studies, the Osh4 protein is comprised of three distinct regions known as mouth containing the ALPS motif and ß6-ß7 connector (red in Figure 1), distal region comprising the ß14- ß15 loop and ß16- ß17 loop (green in Figure 1) and crease section with phenylalanine loop and ß-crease region (blue in Figure 1). To generate the initial system setup for simulations, we have initially oriented the protein in three different ways (mouth, distal and crease) to avoid any bias in results and we have described them accordingly, e.g., donor-mouth system implies the protein is initially placed with the mouth facing the donor membrane surface. To elucidate the membrane binding events of Osh4, we have further divided our study into two sections (i) using HMMM to unravel the effect of membrane fluidity and lipid packing on the binding mechanism of Osh4 and (ii) using AA lipid membrane representation to unravel how the new CUFIX force field parameters modify the overall dynamics of this protein. The simulation details of each system and their replicas are provided in Table S2. The AA simulations without HMMM were carried out for 1000 ns. Whereas, each replica of the HMMM systems were initially run for 300 ns or until membrane-bound conformation is reached (whichever is earlier) and then these were converted to the AA representation and simulated for further 150 ns to refine results obtained from HMMM model to the more realistic in AA model. However, the HMMM simulations were also used to verify that this simplified method can lead to the same bound state with a reduced computational cost as compared to running simulation with all-atom lipid tails. We have discussed the finding of each system in the two different membrane models simultaneously and we will also highlight their key differences. From this point onwards, AA and HMMM terminology represent all-atom and HMMM membrane model, respectively while AA_{HMMM} refers to all-atom lipid membrane representation converted from HMMM . For HMMM systems, the initial binding process of the protein was studied using simulation data from HMMM

while all other analysis at membrane-bound state of the protein, were carried out with the AA_{HMMM} results.

Spontaneous Membrane Binding of Osh4:

The membrane association process of Osh4 involves occasional binding and unbinding events to the membrane surface until the protein reaches a stable binding conformation. We have analyzed the minimum distance profile between protein and membrane with Figures 2A-C representing HMMM, while Figures 2D-E constitute of AA. We have observed that Osh4 binds to the donor membrane for both the HMMM and AA membrane models. As can be seen from Figure 2A, at the beginning, the minimum distance fluctuates rapidly, then, it gradually decreases as the protein approaches the membrane and finally it reaches a plateau with a value of ~3 Å for all donor systems indicating a stable bound conformation. While the minimum distance profiles for donor-crease and donor-mouth runs equilibrate quickly at ~100 ns, the donor-distal requires a longer time to reach the plateau (~260 ns). Figure 2D also shows similar trend along with some occasional fluctuations as observed for AA donor-distal system. Figure 3 represents the adsorption snapshots for Osh4 to the donor membrane along the progress of the simulation for both the HMMM and AA representations.

We have quantitatively analyzed the structural characteristics of the bound state conformations for all the systems. As the Osh4 has three distinct surfaces, namely, mouth, distal and crease, we have calculated the relative position of this membrane binding regions of Osh4 along Z axis with respect to the phosphate-plane of membrane. We have selected a particular residue from each domain, e.g., LYS-15 from mouth, PHE-239 from crease and LYS-258 from distal end, which are representative of individual regions and calculated their relative position of the CA atom with respect to the membrane P -atoms. Inclusion of other residue or the full region (ALPS, ß6-ß7 connector, ß14-ß15 loop, ß16-ß17 loop or phenylalanine loop) provides similar trend. Table S3 lists the relative positions of the selected residues with respect to the membrane surface for all systems. As can be seen from Table S3, the PHE-239 residue shows minimal fluctuations in the bound conformation as it approximately resides within -3 to +2 Å with respect to the membrane P-atoms. The distal region, i.e., LYS-258 was found to reside within ~ 12 to 19 Å whereas the

position of ALPS motif varies moderately among different bound conformations. Furthermore, we have observed a clear trend based on position of PHE-239 residue in bound versus non-bound conformation as PHE-239 was found to lie in close proximity to the membrane P-plane (within -3 to +2 Å) for all bound conformations. For systems that could not produce stable binding (like, acceptor membrane) the relative position of these regions are far away from the membrane surface. Thus, a bound conformation can be defined when the relative position of all three regions falls within stabilized values defined by this crease orientation and thus, fulfilling only one region of the three indicates transient interaction from a particular region of the protein.

We have carefully examined the membrane bound conformation of Osh4 with the donor membrane and a single binding conformation has been observed (Table S3) for all our simulations irrespective of the initial orientation of the protein. As can be seen from Figure 3, in the membrane bound conformation the crease region of the protein lies parallel to the membrane surface as it extends the phenylalanine loop through the membrane surface and establishes contact with the lipid headgroups through its various residues located at different sections of mouth, distal and crease regions. Furthermore, we have also examined how different parts of Osh4 approaches the membrane and facilitate the membrane association process. Figures S1 and S2 show the minimum distance plots of ALPS motif, ß6-ß7 connector, ß14- ß15 and ß16- ß17 loop, phenylalanine loop and ß-crease section for donor-mouth at HMMM and AA membrane representations and all of them show similar characteristics as with the full protein plot. We have found that the minimum distance between the phenylalanine loop and membrane falls rapidly and reaches an equilibrium value of ~3 Å, while for other parts of the protein fluctuation in distance decreases significantly as membrane bound conformation is established. We have also observed that if the distance between the phenylalanine loop and membrane fluctuates (less stable interaction), the protein goes off from the membrane surface at that time frame as reflected in the full protein plot and visual inspection suggesting the general importance of the phenylalanine loop to stable binding.

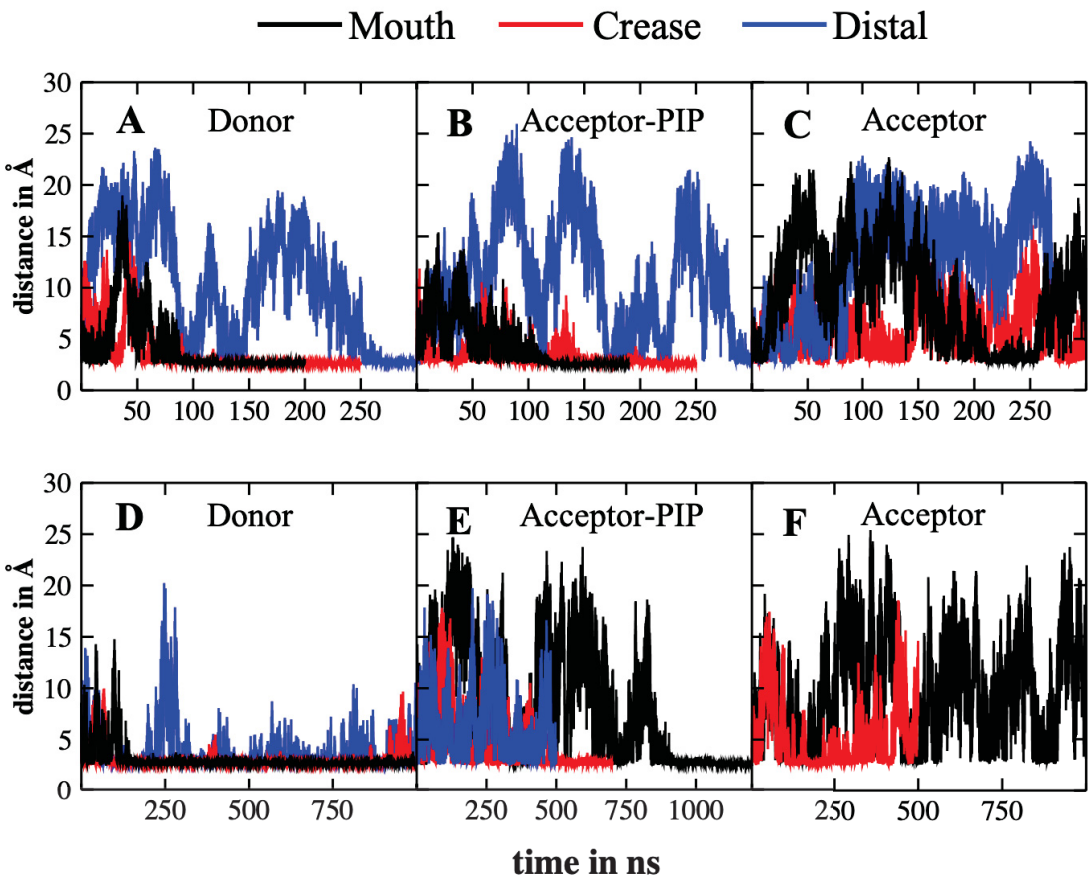

Figure 2: Minimum distance plot between the model membranes and Osh4 for: (A) Donor, (B) Acceptor-PIP and (C) Acceptor systems at HMMM representation, (D) Donor, (E) Acceptor-PIP and (F) Acceptor systems at AA representation.

The acceptor-PIP membrane shows similar trend and we have observed stable binding for two runs (acceptor-PIP-mouth and acceptor-PIP-crease) at the HMMM level within the simulation timescale but AA acceptor-PIP-mouth and acceptor-PIP-crease replicas require much longer timescale to reach stable bound conformation (~850-900 and ~500 ns, Figure 2E). Figure S3 represents the adsorption snapshots for Osh4 at the acceptor-PIP membrane. The structural characteristics at the membrane bound conformation is comparable to the donor system. On the other hand, we could not observe any favorable binding conformation for acceptor membranes at both HMMM and AA levels. Although the protein forms intermittent contacts throughout the simulations, these contacts do not lead to any long-time stable binding (Figures 2C, F).

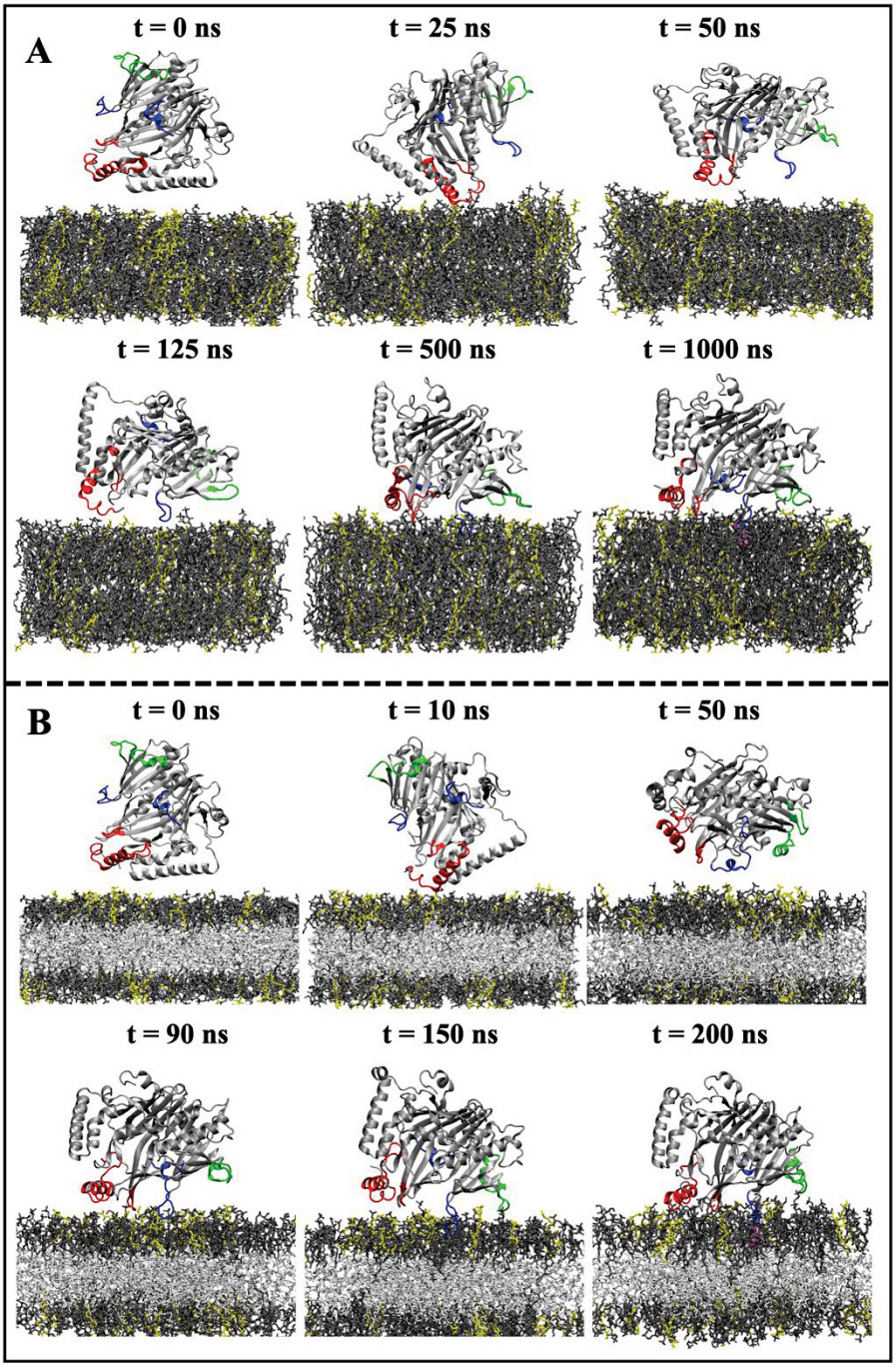

Figure 3: Binding mechanism of Osh4 to the Donor membrane using (A) AA and (B) HMMM membrane models. The color codes for the protein are following: Osh4 in silver, ALPS motif and ß6-ß7 connector in red, ß14-ß15 loop and ß16-ß17 loop in green, phenylalanine loop and ß-crease regions in blue. The PHE-239 residue is shown in VDW representation colored in mauve Zwitterionic lipids are shown in gray and anionic lipids are highlighted in yellow. DCLE molecules are shown in white. Solvent is simulated but not shown.

The initial contacts formed between the protein and membrane and the binding timescale is largely correlated with the initial orientation of the protein with respect to the membrane surface. As we analyze the time evolution of the simulation, we have observed that initially the protein makes non-specific contacts with the lipid headgroups and slowly rotates itself so that it can point the phenylalanine loop towards membrane. As a favorable conformation is reached, the phenylalanine loop penetrates the membrane surface and contacts formed by other regions follow. The binding timescales are calculated to be 100 ns and 90 ns for donor-mouth and donor-crease runs respectively at the HMMM level (125 and 90 ns in AA) while the same for donor-distal is 260 ns. This is because of less rotation required for the protein when it is placed in mouth/crease orientation to reach favorable binding conformation compared to distal orientation. Figure 4 represents the total heavy-atom contacts formed between the protein and membrane before binding for donor systems at the HMMM level. As can be seen from Figure 4, initial interactions are dominated by residues from the ALPS motif and the ß6-ß7 connector for donor-mouth and donor-crease systems and this attractive force acts as driving factor resulting favorable binding of the protein. The ALPS motif is amphipathic in nature and possesses multiple polar residues and further analysis reveals that GLN-3, SER-6, SER-7, THR-11 and LYS-15 from ALPS motif and LYS-173 and SER-174 drive the initial interaction. Similarly, for donor-distal system, as the distal region is pointed towards the membrane, the initial interaction begins from ß16- ß17 loop and the negatively charged carboxylate side chains of GLU-284 and GLU-285 residues form salt-bridge interactions with the positively charged amine moieties of PC/PE/PS lipid head groups driving the process of binding. Similarly, the preliminary interactions for acceptor-PIP systems are also dependent on the initial protein orientation as can be found from Figure S4.

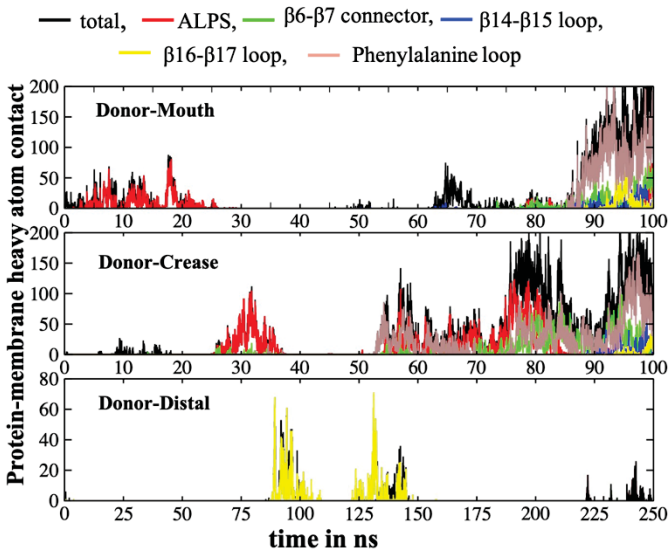

Figure 4: Time evolution of number of contacts between heavy-atoms of protein and membrane (cutoff 5 Å) for donor system using HMMM membrane model.

Analysis of membrane-bound conformation:

Once Osh4 reaches a stable binding conformation, we have analyzed the importance of individual residues towards the membrane association process by computing the frequency of contact between residues and membrane heavy atoms. Frequency of contact (FOC) represents how frequent a particular residue lies within a specified cutoff of heavy atoms of the lipid headgroups. Figure 5 depicts the FOC for donor and acceptor-PIP systems at the AA$_{HMMM}$ level and the same at AA level is shown in Figure S5. Figures 5C and D highlight regions that form close contact > 50% of the time (binding regions with proper residue numbering is provided in Table S4). We have observed similar trend for donor systems at both AA$_{HMMM}$ and AA levels and thus we have discussed the AA$_{HMMM}$ findings thoroughly here. Our analysis reveals multiple regions of Osh4 (namely, ALPS motif, ß6-ß7 connector, ß14- ß15 loop, ß16- ß17 loop and phenylalanine loop and few other residues) form occasional contact with the membrane heavy atom at the bound state. For all donor systems the common factor is that the phenylalanine loop possesses the highest contact frequency indicating membrane proximity of this loop as their overall probability of lying close to the membrane is > 95% throughout the binding event. Apart from this, LYS-173 and SER-174 from ß6-ß7 connector and LYS-283 from ß16- ß17 loop are also found to form close contact >50% of the simulation time. Lastly, the extent of participation from the ALPS motif differs significantly

among donor systems. As for donor-mouth and donor-distal runs, the ALPS motif establishes contact less frequently and LYS-15 acts as a primary interaction site. While for donor-crease run, this motif is involved in much stronger association with lipid headgroups and lies >90% of time close to the membrane.

Similarly, for the acceptor-PIP system at the AA_{HMMM} level, we have observed comparable contact frequency for most of the residues resulting stable membrane attachment of the protein except the ALPS motif. In this case, we have noticed much stronger association of the ALPS motif as their COF peak reaches the value of ~1 for both the runs. The membrane bound conformation (Figure 5D) also supports the fact as the ALPS motif has been found to lie within the membrane having the hydrophobic surface exposed to the membrane core. Interesting, sharp COF peaks at LYS-108 and VAL-208 also result because of stronger ALPS interaction which eventually pulls these residues down into the membrane. The acceptor system does not show any large peaks as it only forms intermittent contact with the membrane via non-specific interactions.

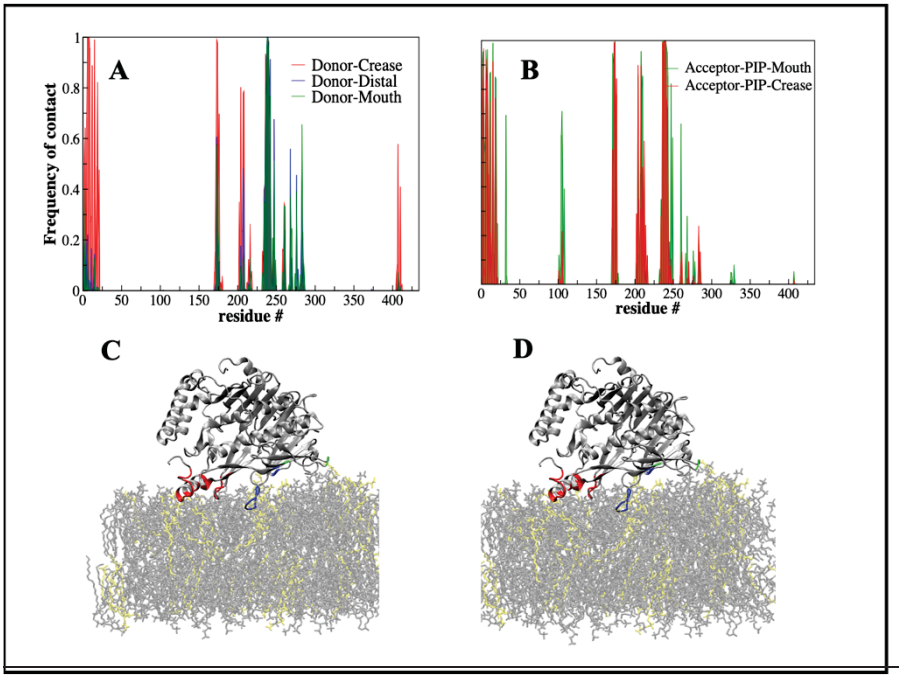

Figure 5. Percentage of time Osh4 residues are within 5Å of the membrane surface for: (A) Donor and (B) Acceptor-PIP using AA_{HMMM} model. Osh4 residues that form close contact > 50% of the time are highlighted for (C) donor and (D) acceptor-PIP systems. The full protein is shown in silver

and the residues forming contact >50% of the time are highlighted in respective region-specific coloring . The membrane is shown in transparent format.

Quantitative structural analysis and visual inspection of the membrane bound conformations for AA (Figure 6A) and AA_{HMMM} (Figure 6B) acceptor-PIP systems reveal that both of them possess similar bound conformation with the protein lying in β-crease orientated fashion with comparable distances for the distal and crease regions of the protein from membrane surfaces. However, the ALPS motif was found to lie in close proximity with the membrane P-atoms for AA_{HMMM} scenario as the relative positions of LYS-15 are 2.7±0.4 and 11.8±0.5 Å at AA and AA_{HMMM} model respectively from the membrane P-atoms. Figure 6 represents the simulation snapshots at both scenarios which clearly depicts the proximity of the ALPS motif to the membrane surface in the AA_{HMMM} scenario. Thus, depending on the association of the ALPS motif with membrane lipids, we have further subcategorized the β-crease bound conformation into two classes (i) bound state I: where ALPS is interacting less frequently as shown in Figure 6A and (ii) bound state II: where ALPS is involved in stronger association with the membrane as in Figure 6B. These are sub types of β-crease membrane bound conformation depending on ALPS association, which were labelled to better understand how the various properties of the bound conformation differs by the extent of ALPS involvement. We have used this classification for rest of the manuscript.

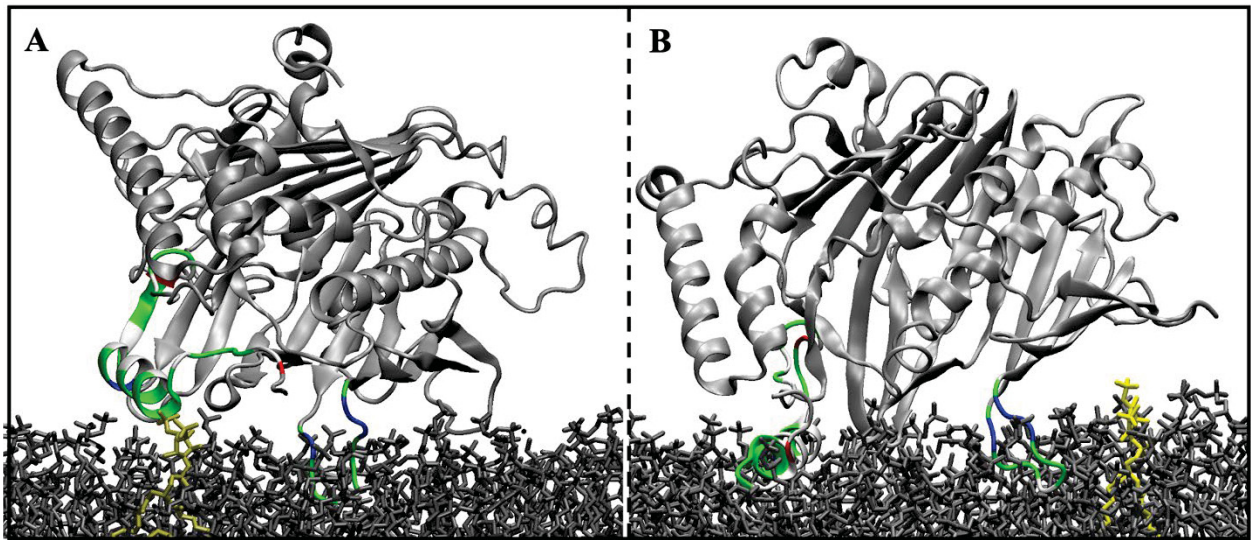

Figure 6. Membrane-bound conformation of Osh4 and position of ALPS motif for acceptor-PIP system: (A) all-atom and (B) AA_{HMMM} membrane models. Color coding is as follows; silver: Osh4, grey: membrane, POPI25 is highlighted in yellow and ALPS motif and phenylalanine loop are shown in residue specific coloring where green: polar, white: non-polar, red: acidic, and blue: basic.

Furthermore, we have compared our computational findings with experimental cysteine-replacement cross-linking studies. Schulz et al.(23) has prepared several single-cysteine mutants to verify how various parts of Osh4 establish contact with the membrane via cross-linking. A protein gets crosslinked to the membrane only when a cysteine comes within ~10 Å of the membrane surface. Schulz et al. identified total nine residues (S8C, A169C, S174C, D191C, G241C, E261C, E284C, N330C, and E412C) which show significant cross-linking during the experiment.(23) We have extended our analysis to include all the residues that lie within 10 Å of the lipid head groups. We have observed that five residues i.e., S8 from ALPS motif, S174 from ß6-ß7 connector, G241 from phenylalanine loop, E261 from ß14-ß15 loop and E283 from ß16-ß17 loop, interact strongly with the membrane and reside >50% of time within specified cutoff for both donor and acceptor-PIP bound states at AA_{HMMM} level. The A169 residue forms occasional contact showing proximity 8% and 35% of time for donor and acceptor-PIP systems respectively. Also, the N330 residue for acceptor-PIP and E412 for donor contacted the membrane 35% and 8% of the time. No significant peaks were observed for those residues that did not crosslink

experimentally (N63C, S76C, K126C, H144C, E306C, E341C, E373C, S389C, and E248C). Lastly, no observable peaks for acceptor system exist as it forms brief contacts with the membrane.

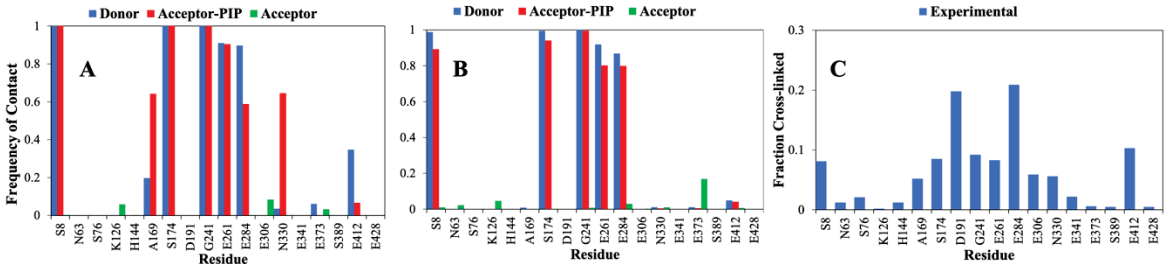

Figure 7. Fraction of time selected Osh4 residues lie within 10Å of the membrane surface calculated for the bound state of the protein: (A) AA_{HMMM} and (B) AA membrane models and (C) fraction of cysteine-mutated protein that is cross-linked with a membrane from the experimental studies of Schulz et al.(23) The FOC is calculated over ~ 500 ns simulation time for AA donor runs, ~300 ns for acceptor-PIP run and last 500 ns for acceptor run. While the same at AA_{HMMM} was calculated for last 150 ns simulation time.

Structural Stability and Penetration of Phenylalanine loop:

Analyzing the membrane-bound conformation of Osh4 reveals that the penetration of the PHE-239 residue is a common trend for all systems at both the HMMM and AA membrane representations. The root mean square deviation (RMSD) was calculated to unravel the structural changes of the phenylalanine loop upon binding. Figure S6 represents the minimum distance of the C_α atoms of residues 239 and 247 (shown in black), RMSD profile of phenylalanine loop (shown in red) and superimposed structures of Osh4 for HMMM donor-mouth and acceptor-PIP-mouth replicas. Figure S6 depicts that the RMSD values of the phenylalanine loop ranges from 3−4Å for all systems Additionally, superimposition of membrane bound conformation with starting Osh4 structure indicates that the loop structure is similar in two scenarios, however its relative placement with respect to neighboring protein residues has changed over time. Initially the phenylalanine loop was inclined towards neighboring ß-sheet comprising residue 245 to 252 (marked in green in Figure S6) and the minimum distance between C_α atoms between residue 239 and 247 was found to be ~10Å. Whereas, as simulation progresses the phenylalanine loop extends itself away from that region resulting a minimum distance of ~20 Å. Furthermore, we have calculated the relative position of PHE-239 residue with respect to membrane phosphate (P)-atoms and Figures 8 and S7 represent the relative Z-position of phenylalanine loop and PHE-239 residue

for donor and acceptor-PIP systems at both the AA$_{HMMM}$ and AA levels. As can be seen from Figures 8A and B, the average position of the PHE-239 residue remains below that of membrane P-atoms for majority of the time indicating stable binding. Whereas for all-atom donor-distal run shows some occasional fluctuation in the position of PHE-239 residue (Figure S7). Thus, the detachment of the phenylalanine loop from the membrane core is accompanied by unbinding of the protein from the membrane surface resulting in a sharp decrease of the protein-membrane interaction energy. Similarly, for the AA acceptor-PIP-mouth system, initially the PHE-239 residue positions itself above the membrane P-atoms up to ~900 ns and as protein reaches stable bound conformation its position falls below that of membrane P-atoms and maintains that position. We have quantitatively measured the penetration depth of PHE-239 residue by calculating its electron density profile. As can be seen from Figure S8, the PHE-239 residue was found to reside ~1 Å and ~4 Å below the membrane phosphate plane for AA$_{HMMM}$ donor and acceptor-PIP systems, respectively.

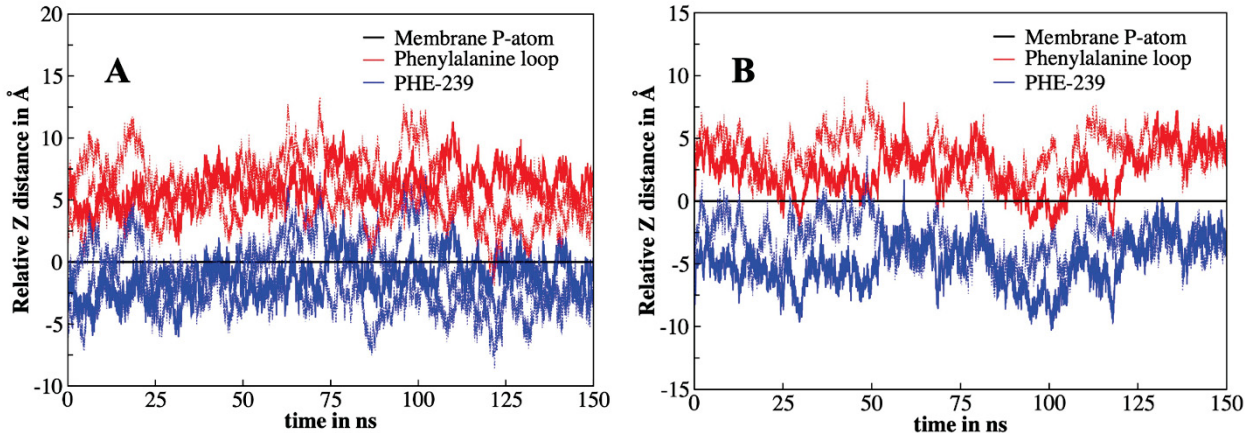

Figure 8. Average position of phenylalanine loop and PHE-239 residue along z-direction with respect to membrane P-atoms for (A) Donor and (B) acceptor-PIP AA$_{HMMM}$ systems. Here, the relative positions are plotted only for the AA$_{HMMM}$ representation after the protein has reached stable bound state and for simplicity, we have labelled the starting as zero and subsequently plotted the rest of the bound state data. The solid line represents mouth replicas whereas crease and distal replicas are shown in dotted line for both systems.

Protein-Membrane Interaction Energy:

The interaction energy (ΔE) between protein and membrane was computed as Osh4 reaches the membrane-bound conformation. This accounts for the enthalpic contribution to the overall free energy of binding. Table 1 lists the protein-membrane interaction energy for all studied systems at both AA_{HMMM} and AA levels and we have included only those systems for which stable binding was observed as for other systems without any stable membrane-attachment the interaction energy was calculated to be negligible. The van der Waals and electrostatic components of the total interaction energy are listed in Table S5. The contribution of individual binding region of Osh4 to the total interaction energy is also listed in Table 1.

Two sets of values for the interaction energy in the membrane-bound state of the protein are observed. For the first set which corresponds to bound state I, the interaction energy ranges from ~ -120 to -150 kcal/mol while for the second set, i.e., bound state II, it ranges from -260 to -360 kcal/mol. Further analysis reveals that for most of the donor runs (three from AA and two from AA_{HMMM}), the interaction energy falls in the first category and only for the donor-crease run at AA_{HMMM} level the ΔE was found to be -267.2 kcal/mol. On the other hand, both the acceptor-PIP runs (acceptor-PIP-mouth and acceptor-PIP-crease) at AA_{HMMM} level belong to the second category as they possess ΔE value of -367.8 and -266.2 kcal/mol, respectively. The major difference between the two categories arises from the contribution of ALPS motif. For bound state I, where the ΔE ranges from ~ -120 to -150 kcal/mol, the phenylalanine loop shows the highest contribution to the overall interaction energy and the ΔE value ranges from ~ -55 to -75 kcal/mol. The van der Waals and electrostatic components of this loop show comparable contributions to the total ΔE. The other binding regions namely, ALPS motif, ß6-ß7 connector, ß14- ß15 loop, ß16-ß17 loop of Osh4 possess moderate ΔE value ranging from -5 to -15 kcal/mol in this category. While for bound state II, we have observed a remarkable increase in the contribution of ALPS motif to the overall ΔE. The ΔE value of this motif ranges from -82 to -125 kcal/mol which is much higher compared to bound state I, but no clear trend in their van der Waals and electrostatic components. The contribution of the phenylalanine loop remains similar or marginally increases from the first category. The stronger association of ALPS motif also engages ß6-ß7 connector more strongly and its contribution in total binding energy increases significantly to ~ -30 to -42 kcal/mol. The remaining parts of the protein namely, ß14- ß15 loop, and ß16- ß17 loop, show a similar trend and their ΔE ranges from ~ -2 to -15 kcal/mol. Thus, our findings indicate that the

overall binding energy does not depend on the charge of the membrane, as we have observed the highest ΔE value for acceptor-PIP system.

We have carefully examined the membrane-bound conformation for both the cases and found that the extent of association of the ALPS motif governs the overall binding energy. Surprisingly, all the systems that have generated higher binding energy, belong to the HMMM category. Thus, loose lipid packing and higher degree of lipid mobility facilitate ALPS to interact more strongly with the membrane.

We have dissected the role different lipids towards overall binding of Osh4, the contribution of individual lipid type towards total membrane-protein interaction energy (ΔE) is computed and tabulated in Table S6. We have further extended these calculations for selected binding region of Osh4 e.g., phenylalanine loop and ALPS motif to understand whether any specific kind of lipid is responsible for stabilizing the interaction between membrane and that region of Osh4. As can be seen from Table S6, for all donor membranes, the contribution from anionic lipids, i.e., POPS and PI(4,5)P2, accounts for approximately ~20 to 35% of the total ΔE value which is much higher compared to its mere concentration (donor membrane has 10% anionic lipid). While the zwitterionic lipids, i.e., POPE, DOPE and POPC contributes ~ 65 to 75% to the overall binding energy. The phenylalanine loop also shows similar behavior and the contributions from zwitterionic or anionic lipids differ marginally as compared to full protein. One the other hand, the acceptor-PIP membrane possesses only one anionic lipid per leaflet, therefore, the interaction between PI(4,5)P2 and protein fluctuates rapidly across simulation width. In few scenarios e.g., AA and AA_{HMMM} Acceptor-PIP-mouth replicas, a single PIP2 lipid contributes 12-25% to the total ΔE value whereas for other case, e.g., AA_{HMMM} Acceptor-PIP-crease replica, it does not form any significant contact within the simulation timescale. Thus, majority of stabilization of the membrane bound conformation for acceptor-PIP system comes from zwitterionic lipids with varying proposition of PC and PE lipids.

Table 1: Protein-Membrane interaction energies for full protein and contribution of selected binding region of Osh4 towards total interaction energy. All values are in kcal/mol. The standard errors are calculated using 10-ns block averages after stable binding.

		Donor			Acceptor-PIP	
		Donor-Mouth	Donor-Distal	Donor-Crease	Acceptor-PIP-Mouth	Acceptor-PIP-Crease
Total	AA_{HMMM}	-134.49±5.33	-128.8±4.27	-267.19±11.98	-367.79±10.04	-266.22±6.89
	AA	-135.22±4.7	-41.45±3.46	-118.33±7.43	-132.61±7.52	-106.38±8.01
ALPS motif	AA_{HMMM}	-4.90±0.95	-5.481±1.14	-108.79±6.23	-125.27±3.39	-82.09±4.39
	AA	-4.45±0.59	-2.15 ±0.48	-32.10±4.05	-37.91±5.06	-2.64±1.28
β6-β7 connector	AA_{HMMM}	-11.42±1.75	-8.38±1.03	-42.82±3.14	-32.51±1.64	-33.69±1.97
	AA	-11.85±1.29	-4.92 ±1.23	-7.69±0.75	-6.30±1.27	-8.1±1.79
β14-β15 loop	AA_{HMMM}	-7.19±1.16	-4.48±1.1	-7.52±1.99	-12.55±1.98	-1.98±0.47
	AA	-6.25±0.71	-3.13 ±0.64	-4.77±1.10	-4.16±1.12	-5.30±0.91
β16-β17 loop	AA_{HMMM}	-9.62±1.14	-6.23±1.23	-1.17±0.44	-2.79±0.55	-3.48±0.61
	AA	-9.46±0.94	-5.15±0.98	-9.98±1.13	-6.25±0.70	-6.99±2.09
Phenylalanine loop	AA_{HMMM}	-74.90±3.43	-75.16±1.51	-64.32±4.10	-103.89±3.49	-85.64±2.14
	AA	-74.62±2.51	-21.62±2.60	-55.32±3.85	-67.49±2.73	-67.58±3.75

Protein-Membrane Categorized Interactions:

The association of a peripheral membrane protein to the membrane surface involves various types of specific and non-specific electrostatic and hydrophobic interactions among which hydrogen-bonding (h-bond) and salt-bridges are common. In h-bonding, a covalently attached polar h-atom engages in dipole-dipole attraction with another electronegative atom which is primarily held together by electrostatic forces of attraction. While, salt-bridge interactions are formed between ion-pairs and it is a combination of two non-covalent interactions, h-bonding and ionic interactions. Salt bridge interactions occur as two heavy-atoms of opposite charge, namely, N^+ from LYS sidechain and O^- from lipid head group, fall within h-bonding distance. Charged amino acid side chains namely, LYS, ARG, GLU and ASP, engage in salt-bridge interactions more frequently with lipid head groups. We have calculated the salt-bridge and h-bonding pattern between the protein and membrane for all membrane-bound conformations. The contribution of both the backbone and the sidechain residues towards overall bonding are considered. Figure S9 represents the total number of h-bonds formed between protein and membrane during the

simulation for the donor and acceptor-PIP systems at both the AA_{HMMM} and AA levels, respectively. We have analyzed the details of h-bonding once membrane-bound conformation is reached. As total h-bonding count also includes a fraction of salt-bridge interactions, we have deducted the salt-bridge interactions proportionally to get the sole h-bonding count. Initially the protein forms h-bonds less frequently for both donor and acceptor-PIP systems which eventually increase as the membrane bound conformation is reached. On average, all the donor systems possess 1 to 2 h-bonds except the donor-crease run at AA_{HMMM} level which was found to form 3 to 4 h-bonds at a given timeframe. Similarly, the acceptor-PIP runs at AA_{HMMM} level are also found to form more frequent h-bonding compared to its AA level counterpart. Thus, detailed analysis reveals that, on average, the protein forms two to three more h-bonds in bound state II compared to bound state I for all systems. This classification of bound state is similar to previous section and our h-bonding pattern also follows similar trend. For bound state I, the phenylalanine loop accounts for >45-85% of the total h- bonds and residues namely, TYR-238, backbone of PHE-239 and SER-240 form majority of h-bonds in this case. Other residues, e.g., SER-2, GLN-3, SER6, SER-8, THR-11 and SER-19 from ALPS motif, THR-172 and SER-174 from ß6-ß7 connector, ASP-259 from ß14-ß15 loop, SER-286 from ß16-ß17 loop, involve in occasional h-bonding with the DOPC/POPS/POPE head groups. On the other hand, for bound state II, where the ALPS motif lies in close association with the membrane, the contribution of ALPS motif and phenylalanine loop towards total h-bonding is comparable and their contribution ranges from 40 to 75% for ALPS motif and 25 to 45% for phenylalanine loop, respectively. Additionally, polar residues from ALPS motif engage more frequently with the membrane resulting higher h-bonds for this conformation. On average, the protein was found to form ~1 to 1.5 salt-bridge interactions for bound state I and ~ 2 to 3 for bound state II at a given timeframe. Several charged residues namely, LYS-15 from ALPS motif, LYS-173 from ß6-ß7 connector, LYS-242 from phenylalanine loop, LYS-260 and GLU-261 from ß14-ß15 loop and LYS-283 and GLU-285 from ß16-ß17 loop primarily engage in salt-bridge interactions with the charged moiety of lipid head groups.

We have also calculated the heavy atom contacts formed between protein and the membrane at the membrane bound state as this will account for all other types of interaction. Percentage of contact formation by a specific lipid type is tabulated in Table S7. Figures S10A and B represent the heavy atom contacts made by Osh4 to the membrane heavy atom and Figures S10C and D represent the

number of heavy atom contacts formed by the hydrophobic residues of ALPS motif in acceptor-PIP systems. We have observed similar trend with h-bonding pattern and the contribution of individual regions towards total contact formation is dependent on the type of bound state. For bound state I, phenylalanine loop possesses 75 to 80% of the total contacts while the same for bound state II is ~ 30%. In bound state II, the ALPS motif possesses ~ 40% of the total contacts formed by this protein. As can be seen from Table S7, the contact formation between protein and membrane are dominated by zwitterionic PC and PE lipids. We have further investigated how the hydrophobic residues of ALPS motif establishing contact with the membrane in two different scenarios and Figures S10C and D represent the total heavy atom contact formed by ALPS motif along with its hydrophobic residues. We have found that the contacts formed by hydrophobic residues has increased to 33% for bound state II as compared to 7% in bound state I, bound state I which further validates the stronger engagement of this motif at membrane surface.

Discussion:

Our computational studies have identified that the Osh4 protein binds to membranes with at least one anionic lipid per leaflet for both AA and HMMM representations. The acceptor membrane with solely zwitterionic lipids was unable to form stable contact with Osh4. Contacts with this membrane occur but only transiently (limited to 10-40 ns) as shown in Figures 2C and F. While systems with anionic lipids, at both AA and HMMM representations, have generated a single membrane bound conformation in which the protein lies on its side with ß-crease region facing the membrane and the phenylalanine loop penetrated inside membrane (Figures 3 and S3). The membrane association process of Osh4 occurs in a stepwise manner. Initially, non-specific attractions between lipid headgroups and amino acid sidechains drive the process and the preliminary interactions between them is guided by the orientation of protein at the membrane surface (Figures 4 and S4). Thus, when the protein is placed in the mouth or crease orientation, the ALPS motif and ß6-ß7 connector located at the mouth region of the protein start to interact non-specifically with the lipid headgroups through its polar residues, while, for distal-oriented Osh4, anionic GLU residues of ß16-ß17 loop guide the initial attraction. Subsequently, as can be seen from Figure 3A, the protein gradually rotates itself following 25-125 ns in such a way, so that the crease region of the protein lies parallel to the membrane surface. The rotation timescale varies

moderately among various systems, as for AA donor-mouth run (Figure 3A), the rotation begins at ~25 ns and reaches the crease orientation at ~125 ns, while the same for the HMMM level are ~15 and 90 ns (Figure 3B). Once favorable conformation is achieved, the phenylalanine loop extends itself (~125 ns for AA donor-mouth at Figure 3A) towards membrane core and penetration of PHE-239 is the final landmark of stable membrane attachment of Osh4. Then, different residues located at ß6-ß7 connector, ß16-ß17 loop, ß14-ß15 loop and ALPS motif maximizes their interaction with the lipid headgroups stabilizing the bound state. Although the binding time scale and rotation time vary from system to system, the overall mechanism of membrane association is similar for all acceptor-PIP and donor systems at both AA and HMMM levels (Figures 3 and S3). Figures 8 and S7 show that the PHE-239 residue lies below that of the phosphate plane for majority of the simulation time at membrane bound state and fluctuation in position of PHE-239 also gets reflected to other parts of the protein. Interestingly, the penetration of the PHE-239 below phosphate plane is crucial for stable membrane attachment of this protein and we have observed that as this residue detaches from the membrane surface, the protein is also unable to maintain stable attachment and is rapidly released from the membrane.

Our current observation of single membrane-bound conformation complies with our previous computational study(32), however the degree of participation of various residues towards overall binding is different. Rogaski et. al. (32) observed similar membrane bound conformation of Osh4, where the protein is positioned in ß-crease fashion, however, the course of membrane association is different. Rogaski et al. proposed that after initial rotation of the protein to crease orientation, several basic residues located at ß14-ß15 and ß16-ß17 loops establish the initial contact with the acidic lipid headgroups followed by interactions from mouth region of Osh4, i.e., ALPS motif and ß6-ß7 connector and finally the C-terminal β-crease region binds to the membrane. No specific trend for membrane attachment of the phenylalanine loop was observed, as it might occur before, during or after other regions of Osh4 establish stable contact with the membrane.(32) Thus, the key difference between two mechanism is the participation and importance of the phenylalanine loop to overall binding of the protein. We have found (Table 1) that this loop is very crucial for maintaining the membrane-bound conformation of Osh4 and it accounts for ~ 25-60% of the total protein-membrane interaction energy. While, the contribution of this loop as observed in the past work of Rogaski et. al. only ranges from 15-20% of the total interaction energy. Moreover, we

could not observe any significant interaction from the ß-crease (402 to 413) region of Osh4. The increased importance of phenylalanine loop is likely due to the use of a more balanced force field for electrostatic/dispersion interactions with CUFIX (more details below).

The amphipathic lipid packing sensor (ALPS) motif has been shown to sense membrane curvature and lipid packing.(52) Heavy-atom contact analysis (Figure S10) between protein and membrane and simulation snapshots (Figure 6) show that in the membrane bound state the engagement of ALPS motif with the lipid head groups differs in two membrane models. We have classified these two states as bound state I, where the ALPS motif lies parallel to the membrane surface (Figure 6A) and interacts mostly with its polar residues via electrostatic manner and bound state II (Figure 6B), where the ALPS motif is strongly adsorbed on the membrane surface and the hydrophobic residues of this motif establish contact more frequently with the membrane along with its polar residues. Thus, in bound state II, the ALPS motif acts as strong gluing point compared to bound state I. We have observed bound state I for all donor and acceptor-PIP simulations with AA membrane representations. Whereas, two HMMM runs of acceptor-PIP system and donor-crease run at the HMMM level have generated protein conformation in bound state II. The ALPS motif is amphipathic in nature and possesses both polar and hydrophobic faces on opposite sides of the helix. Hence, the degree of interaction by this motif is governed by its orientation at the membrane surface. Visual inspection of the simulation snapshots and estimation of hydrophobic contact (Figure S10) suggest when the hydrophobic part of the is motif is positioned downwards facing the membrane a stronger association occurs compared to the reverse scenario. The donor-crease run, acceptor-PIP-mouth and acceptor-PIP-crease runs for the HMMM representation resulted in conformations where the hydrophobic regions of the ALPS motif is facing downward prevailing close proximity of the overall motif to the membrane. While, for other membrane-bound systems, we have observed that the ALPS motif lies parallel to the membrane surface and involves in contact less frequently compared to the previous case. As per Table 1, the protein-membrane interaction energy also validates these two bound states. For bound state I, the binding energy ranges from -120 to -150 kcal/mol and the phenylalanine loop contributes significantly to the overall binding (>50% of the total binding energy). While for bound state II, the ΔE value ranges from -260 to -360 kcal/mol and the ALPS motif contributes significantly towards total binding energy and in few cases its contribution exceeds that of phenylalanine loop. For a majority of the scenarios, both

contribute almost equally to the overall binding. Heavy atom contact (Figure S10C and D) analysis reveals that enhanced binding from ALPS motif is because of more direct interaction of its hydrophobic face with the membrane resulting stronger association.

Previous all-atom MD simulations exploring the binding dynamics of ALPS motif by Monje-Galvan et al.(53) identified two significant bound conformations of the ALPS peptide, where in the vertical conformation, the N-terminus of the peptide interacts deeply with the membrane hydrophobic core while in the horizontal conformation, the peptide lies parallelly to the membrane surface with its hydrophobic surface embedded into the membrane core. The horizontal conformation was predicted to be the more favorable one in terms of binding energetics and bulky residues namely, PHE-13, TRP-10 and THR-11 was found to facilitate the non-polar interactions with the membrane lipids. Furthermore, the extent of binding was proposed to vary depending on the nature of bilayer and thus, model membranes with higher percentage of anionic lipids and large packing defects favor the binding process of the peptide.(53) Switching from AA to HMMM enhanced the binding timescale of ALPS motif by roughly 1 order of magnitude as shown by Wildermuth et al.(37) The resulting equilibrium conformation at the HMMM level was found to be similar with previous horizontal AA conformation, where the hydrophobic residues of the ALPS motif are orientated towards the membrane surface. In full protein environment, the ALPS motif was predominantly found in horizontal conformation as described above. Although, the ALPS lies parallel to the membrane surface, in bound conformation the orientation of the main helix is significantly different among various systems. For majority of the cases including all AA and few HMMM systems (Figure 6A), the interaction of the ALPS motif is limited to mostly electrostatic interactions among polar amino acid residues and lipid headgroups. However, acceptor-PIP HMMM systems and HMMM donor-crease run has resulted in extended ALPS engagement conformation where hydrophobic residues are in strong association with membrane lipids as shown in Figure 6B. This suggests that the timescales for the AA runs would require an order of magnitude more to observe ALPS penetration into the hydrophobic core similar to what was observed by Wildermuth et al. (37) with the peptide alone. Interestingly, bound state II was found to be energetically more favorable as compared to bound state I suggesting the horizontal placement of ALPS in the membrane is enthalpically preferred. Thus, with the full protein, conformational restrictions by remaining parts of the protein as compared to truncated peptide,

favors horizontal placement of ALPS motif and we believe that with extended simulations the bound state I conformations will eventually evolve into the bound state II conformation.

Experimental studies by Schulz et al.(23) demonstrated that Osh4 can establish contact with two opposing membranes simultaneously. Furthermore, cysteine-crosslinked and NBD fluorescence experiments revealed two distinct membrane binding regions, one located near mouth of the protein while the other located at the distal region of the protein. Total nine residues, five (S8C, A169C, S174C, N330C, and E412C) from mouth region, three from (D191C, E261C, and E284C) distal region and few other residues (E306C, E341C, and G241C) were found to cross-linked with the membrane significantly. E306C, E341C, and G241C residues were located at the crease region. It was proposed while, one end of the protein (i.e., mouth region) establishes contact with one membrane, other end (i.e., distal region) facilitates contact with the opposing membrane, thus, enabling the transport of sterol across them.(23) As we compare our simulation results with experimental cross-linked data, we found that five out of nine residues namely, S8, S174, G241, E261, E284, always lies within 10 Å of the membrane surface for all systems at both AA_{HMMM} and AA representation. In contrast to previous computational findings(32), we could not observe any significant peak for E412 with a majority of systems. Additionally, bound state II of AA_{HMMM} acceptor-PIP system has generated two sharp peaks at A169 and N330 position and these two residues were found to be close to the membrane for 65-70% of the time. Similarly, for AA_{HMMM} donor-crease run at bound state II, residues A169 and E412 were close to the donor membrane for significant amount of time. Also, there were no peaks observed for residues E306 and E341. Thus, stronger association of ALPS motif in bound state II, pulls down the neighboring regions of ß6-ß7 loop resulting the A169 residue in the proximity of the membrane as compared to bound state I. Thus, residue proximity profile for bound state II shows excellent agreement with experiment as 7 to 8 residues were found to be membrane bound. We could not observe any peaks for the D191 residue, located at the distal end of the protein, which was found to be cross-linked significantly in the experimental studies by Schulz et al.(23) The contrast between the experimental and computational proposed binding sites arises from the nature of two studies. Under experimental circumstances, the protein was shown to bind with two liposomes simultaneously and the overall transport process occurs through cascade of steps and therefore, the protein has enough rooms to orient around multiple membrane-bound and unbound conformations. Thus, the cysteine-

crosslinked and NBD fluorescence results represent an average picture of this multistep process. While, our computational studies indicate the initial interaction between Osh4 and model membranes. Moreover, another major difference arises because of environment and timescale of the study. While, the computational study was caried out with single membrane model and limited to only 1000 ns, the same at experimental setup was carried out for 30 mins with multiple liposomes. Hence, we believe that the Osh4 primarily binds to membrane through the ß-crease conformation and subsequently, it undergoes conformational transition specific to its known function as a membrane contact site former simultaneously binding to two liposomes. Thus, our findings suitably represent the initial interactions between the protein and the membrane in a single membrane model environment.

The association of peripheral proteins with lipid membranes are largely governed by the interactions of charged moieties of the protein, i.e., positively charged LYS and ARG, and negatively charged ASP and GLU, with lipid headgroups containing negatively charged carboxylate and phosphate moieties along with positively charged amine group. Yoo et. al. reported a CUFIX parameter that systematically refines the pair-specific Lennard-Jones parameters for amine−carboxylate and amine−phosphate interactions.(30) These improved non-bonded parameters provide better agreement with experimental results without introducing further artifacts. Incorporation of CUFIX force field parameters in our simulations has modified the protein-membrane interactions significantly as several charged residues located at different membrane binding regions of Osh4 were found to form salt-bridge interactions with lipid headgroups throughout the bound conformation. We have primarily observed two sets of binding energies for their respective membrane-bound conformations as discussed previously. According to Table 1, the phenylalanine loop contributes predominantly for bound state I, while, for bound state II, the phenylalanine loop and ALPS motif contribute comparably towards overall binding for majority of scenarios. Other binding regions of Osh4 namely, ß14-ß15 loop and ß16-ß17 loop show similar contributions for both bound states. Previous studies by Rogaski et. al.(32) have shown that the ß14-ß15 loop possess the highest contribution towards total binding energy and it was also proposed that the electrostatic attraction acts as the key factor for stable membrane attachment of Osh4. Although the bound conformation is like the previous all-atom study and importance of various regions of Osh4 towards overall stability of the membrane attachment

process is strikingly different. The new CUFIX force field parameters along with CHARMM36m modifies the non-bonded interactions between the charged groups, i.e., amine-phosphate and amine-carboxylate, of protein and membrane in a more realistic manner and provides a balanced picture of hydrophobic and electrostatic forces for membrane attachment of Osh4. We recommend that simulations with peripheral membrane proteins with cationic residues interacting with anionic lipids to use the new CUFIX modification to better balance electrostatic and dispersive interaction.

The HMMM membrane with large packing defects has been shown to accelerate the binding event of the ALPS peptide because of substantial exposure of the non-polar lipid core which favors the hydrophobic attractions between the two.(37) Switching from AA to HMMM enhances the flexibility and mobility of the lipids by one to two orders of magnitude, which eventually favors the association of membrane-targeting domains with the membrane.(35) We have identified a membrane-bound state (bound state II) where ALPS engages through its hydrophobic regions at the membrane surface and this phenomenon is more predominant for HMMM membranes. Increased lipid diffusion and less packing has enabled stronger association and deeper penetration of the ALPS motif in HMMM membrane environment as compared to AA. Moreover, bound state obtained from the HMMM model, i.e., bound state II, has shown improved agreement with the experimental cross-linking results.(23) The A169 and N330 residues were found to lie close to the membrane for >60% of the simulation time for AA_{HMMM} Acceptor-PIP systems which was clearly absent in AA model. Also, stronger association of ALPS motif has increased the stability of the bound conformation by 2-3-fold as compared to AA. Although, the binding timescales of Osh4 are comparable in both AA and HMMM models for donor systems, we have observed less fluctuations in bound conformation for HMMM representation compared to AA. While, the binding time scale for acceptor-PIP has been found to expedite in HMMM model and for two (mouth and crease) runs binding occurs within 150 ns while the same at AA is > 500 ns. This is likely related to the single anionic lipid in the acceptor-PIP lipid requiring more time to search the surface for non-specific electrostatic interactions in the AA compared to the more dynamic HMMM.

Peripheral proteins bind transiently to the membrane surface and thus, predicting the membrane-bound states and their conformational transitions can be challenging. According to recent studies,

Osh4 is proposed as a sterol/PI(4)P exchanger and its mechanism revolves around transporting sterol from donor to acceptor membrane in exchange of PI(4)P until the effective sterol gradient disappears between the two membranes. Furthermore, it was also predicted that Osh4 can function at MCS where it establishes contact with two opposing membranes simultaneously and transports sterol across them.(17) Each of these sterol uptake and release steps are associated with large conformational changes of the protein as observed in the crystal structure study of Osh4 where sterol release was accompanied by a potential conformational change of α_7 helix during the transport cycle.(21) Experimental studies provide a time-averaged picture of the whole process, while, MD simulations depict a comprehensive picture of individual steps in the sterol transport cycle. In this study, we have utilized all-atom MD simulations to understand the initial binding mechanism of Osh4 with model membranes composing zwitterionic and anionic lipids in single membrane. In contrast to experimental predictions of two membrane binding surfaces, i.e., mouth and distal, we have observed a single membrane bound conformation of Osh4 where it lies with the ß-crease regions facing downwards at the membrane surface. The distinction between the number of experimentally-proposed membrane binding surfaces and computationally predicted one arises because of the nature of two studies. We believe that the primary association between Osh4 and membranes occur through computationally-predicted ß-crease conformation and subsequently the protein undergo conformational transition during the sterol transport cycle. HMMM simulations have resulted in a membrane-bound state (bound state II) where the ALPS motif was found in close association with the lipids through its hydrophobic regions. Moreover, our results show excellent agreement with the experimental cross-linking data(23) and majority of residues cross-linked experimentally were also found to be important for stable binding of Osh4. Thus, the binding mode of different membrane binding regions is regulated by various factors like, membrane composition and curvature, packing defects. Hence, introduction of more complexity in our simulation setup, like membrane curvature and packing defects might impact the binding of the ALPS motif considerably and hence, the bound conformation Osh4. Therefore, we expect enhanced sampling or guided simulations setup along with more realistic representations including dual membranes are required to explore the full function of Osh4 in the sterol and lipid transport cycle.

In conclusion, microsecond long all-atom molecular dynamics simulations were carried out to unravel the membrane binding dynamics of yeast Osh4 protein with both AA and HMMM using the CHARMM36m forcefield parameters along with CUFIX modifications. Our detailed computational studies have identified a single membrane bound conformation of Osh4 for all anionic membranes where it lies in β-crease orientated fashion with its phenylalanine loop penetrated through the membrane surface. Additionally, we have observed a membrane bound state, i.e., bound state II, where the ALPS motif was found in extended engagement through its hydrophobic residues with the membrane lipids. The observation of a single bound conformation agrees well with the previous computational study. Furthermore, binding energy calculations reveal that phenylalanine loop plays a crucial role in stable membrane attachment of this protein and penetration of the PHE-239 residue below the membrane phosphate plane is the final landmark of binding process. Interestingly, the ALPS motif was also found to contribute significantly for overall binding of Osh4 specifically for bound state II resulting stronger association of the protein. Thus, our all-atom molecular dynamics simulations provide a detailed picture of initial interactions of the Osh4 protein with various model membranes in a single membrane model environment. Further advanced computational and experimental studies are required to elucidate the overall mechanism of sterol transport process by Osh4.

Author Contributions:

JBK and SK designed the project. SK carried out the simulations and performed all the analyses. SK wrote the manuscript with contributions from JBK.

Acknowledgements:

All simulations ran on the Extreme Science and Engineering Discovery Environment (XSEDE) (grant # MCB-100139) and Maryland Advanced Research Computing Center (MARCC) supercomputer. Analysis of data was performed on the MARCC supercomputer and University of Maryland's Deeptought2 which is maintained by the Division of Information Technology. This research is supported by the NSF grant MCB-1951425.

Notes:

The authors declare no competing financial interest.

Supporting Information:

The supporting materials include lipid composition of model membranes (Table S1), system description and production run simulation time (Table S2), average distance in between selected residues of Osh4 and the phosphate component of the membrane (Table S3), list of residues forming contact >50% of time (Table S4), protein-Membrane interaction energy and its van der Waals (VDW) and electrostatic (ELEC) components (Table S5), contribution of individual lipid type towards total membrane-protein interaction energy (Table S6), percentage of contact formation by individual lipid type (Table S7), minimum distances between the donor membrane and different region of Osh4 for HMMM (Figure S1) and AA (Figure S2) membrane models, simulation snapshots of binding mechanism of Osh4 to the acceptor-PIP membrane for AA and HMMM representation (Figure S3), time evolution of number of contacts between heavy-atoms of protein and membrane for acceptor-PIP system using HMMM membrane model (Figure S4), frequency of contact of Osh4 residues for Donor and acceptor-PIP systems (Figure S5), minimum distance profile between Cα atoms of residues 239 and 247 and RMSD profile of phenylalanine loop (Figure S6), relative position of phenylalanine loop and PHE-239 residue along z-axis (Figure S7), electron density profile of selected membrane regions and PHE-239 residue (Figure S8), hydrogen bonds for Donor and Acceptor-PIP systems (Figure S9) and number of contacts between heavy-atoms of protein and membrane and contribution of ALPS motif towards total contacts (Figure S10).

References:

1. Cho, W., and R. V. Stahelin. 2005. Membrane-protein interactions in cell signaling and membrane trafficking. *Annu. Rev. Biophys. Biomol. Struct.* 34:119-151.
2. Merz, K. M., and B. Roux. 2012. Biological membranes: a molecular perspective from computation and experiment. Springer Science & Business Media.
3. Stahelin, R. V. 2009. Lipid binding domains: more than simple lipid effectors. *Journal of lipid research*. 50:S299-S304.
4. James, S. R., C. Peter Downes, R. Gigg, S. J. Grove, A. B. Holmes, and D. R. Alessi. 1996. Specific binding of the Akt-1 protein kinase to phosphatidylinositol 3, 4, 5-trisphosphate without subsequent activation. *Biochemical Journal*. 315(3):709-713.
5. Pitcher, J. A., Z. L. Fredericks, W. C. Stone, R. T. Premont, R. H. Stoffel, W. J. Koch, and R. J. Lefkowitz. 1996. Phosphatidylinositol 4, 5-bisphosphate (PIP2)-enhanced G protein-coupled receptor kinase (GRK) activity: Location, structure, and regulation of the

PIP2 binding site distinguishes the GRK subfamilies. *Journal of Biological Chemistry*. 271(40):24907-24913.

6. Lemmon, M. A., K. M. Ferguson, R. O'Brien, P. B. Sigler, and J. Schlessinger. 1995. Specific and high-affinity binding of inositol phosphates to an isolated pleckstrin homology domain. *Proceedings of the National Academy of Sciences*. 92(23):10472-10476.
7. Holthuis, J. C., and A. K. Menon. 2014. Lipid landscapes and pipelines in membrane homeostasis. *Nature*. 510(7503):48-57.
8. Van Meer, G., D. R. Voelker, and G. W. Feigenson. 2008. Membrane lipids: where they are and how they behave. *Nature reviews Molecular cell biology*. 9(2):112-124.
9. Gennis, R. B. 2013. Biomembranes: molecular structure and function. Springer Science & Business Media.
10. Prinz, W. A. 2010. Lipid trafficking sans vesicles: where, why, how? *Cell*. 143(6):870-874.
11. Hanada, K., and D. Voelker (2014). Interorganelle trafficking of lipids: Preface for the thematic review series. Wiley Online Library.
12. Salminen, T. A., K. Blomqvist, and J. Edqvist. 2016. Lipid transfer proteins: classification, nomenclature, structure, and function. *Planta*. 244(5):971-997.
13. Wong, L. H., A. T. Gatta, and T. P. Levine. 2019. Lipid transfer proteins: the lipid commute via shuttles, bridges and tubes. *Nature Reviews Molecular Cell Biology*. 20(2):85-101.
14. Lev, S. 2010. Non-vesicular lipid transport by lipid-transfer proteins and beyond. *Nature reviews Molecular cell biology*. 11(10):739-750.
15. Toulmay, A., and W. A. Prinz. 2012. A conserved membrane-binding domain targets proteins to organelle contact sites. *Journal of cell science*. 125(1):49-58.
16. Schulz, T. A., and W. A. Prinz. 2007. Sterol transport in yeast and the oxysterol binding protein homologue (OSH) family. *Biochimica et Biophysica Acta (BBA)-Molecular and Cell Biology of Lipids*. 1771(6):769-780.
17. Beh, C. T., C. R. McMaster, K. G. Kozminski, and A. K. Menon. 2012. A detour for yeast oxysterol binding proteins. *Journal of Biological Chemistry*. 287(14):11481-11488.
18. Beh, C. T., L. Cool, J. Phillips, and J. Rine. 2001. Overlapping functions of the yeast oxysterol-binding protein homologues. *Genetics*. 157(3):1117-1140.
19. Delfosse, V., W. Bourguet, and G. Drin. 2020. Structural and Functional Specialization of OSBP-Related Proteins. *Contact*. 3:2515256420946627.
20. Ghaemmaghami, S., W.-K. Huh, K. Bower, R. W. Howson, A. Belle, N. Dephoure, E. K. O'Shea, and J. S. Weissman. 2003. Global analysis of protein expression in yeast. *Nature*. 425(6959):737-741.
21. Im, Y. J., S. Raychaudhuri, W. A. Prinz, and J. H. Hurley. 2005. Structural mechanism for sterol sensing and transport by OSBP-related proteins. *Nature*. 437(7055):154-158.
22. Raychaudhuri, S., Y. J. Im, J. H. Hurley, and W. A. Prinz. 2006. Nonvesicular sterol movement from plasma membrane to ER requires oxysterol-binding protein–related proteins and phosphoinositides. *The Journal of cell biology*. 173(1):107-119.
23. Schulz, T. A., M.-G. Choi, S. Raychaudhuri, J. A. Mears, R. Ghirlando, J. E. Hinshaw, and W. A. Prinz. 2009. Lipid-regulated sterol transfer between closely apposed membranes by oxysterol-binding protein homologues. *Journal of Cell Biology*. 187(6):889-903.

24. de Saint-Jean, M., V. Delfosse, D. Douguet, G. Chicanne, B. Payrastre, W. Bourguet, B. Antonny, and G. Drin. 2011. Osh4p exchanges sterols for phosphatidylinositol 4-phosphate between lipid bilayers. *Journal of Cell Biology*. 195(6):965-978.
25. Alfaro, G., J. Johansen, S. A. Dighe, G. Duamel, K. G. Kozminski, and C. T. Beh. 2011. The sterol-binding protein Kes1/Osh4p is a regulator of polarized exocytosis. *Traffic*. 12(11):1521-1536.
26. Kajiwara, K., A. Ikeda, A. Aguilera-Romero, G. A. Castillon, S. Kagiwada, K. Hanada, H. Riezman, M. Muñiz, and K. Funato. 2014. Osh proteins regulate COPII-mediated vesicular transport of ceramide from the endoplasmic reticulum in budding yeast. *Journal of cell science*. 127(2):376-387.
27. Klauda, J. B., R. M. Venable, J. A. Freites, J. W. O'Connor, D. J. Tobias, C. Mondragon-Ramirez, I. Vorobyov, A. D. MacKerell Jr, and R. W. Pastor. 2010. Update of the CHARMM all-atom additive force field for lipids: validation on six lipid types. *The journal of physical chemistry B*. 114(23):7830-7843.
28. Best, R. B., X. Zhu, J. Shim, P. E. Lopes, J. Mittal, M. Feig, and A. D. MacKerell Jr. 2012. Optimization of the additive CHARMM all-atom protein force field targeting improved sampling of the backbone ϕ, ψ and side-chain $\chi 1$ and $\chi 2$ dihedral angles. *Journal of chemical theory and computation*. 8(9):3257-3273.
29. Huang, J., S. Rauscher, G. Nawrocki, T. Ran, M. Feig, B. L. De Groot, H. Grubmüller, and A. D. MacKerell. 2017. CHARMM36m: an improved force field for folded and intrinsically disordered proteins. *Nature methods*. 14(1):71-73.
30. Yoo, J., and A. Aksimentiev. 2016. Improved Parameterization of Amine–Carboxylate and Amine–Phosphate Interactions for Molecular Dynamics Simulations Using the CHARMM and AMBER Force Fields. *Journal of Chemical Theory and Computation*. 12(1):430-443, doi: 10.1021/acs.jctc.5b00967, https://doi.org/10.1021/acs.jctc.5b00967.
31. Ohkubo, Y. Z., T. V. Pogorelov, M. J. Arcario, G. A. Christensen, and E. Tajkhorshid. 2012. Accelerating membrane insertion of peripheral proteins with a novel membrane mimetic model. *Biophysical journal*. 102(9):2130-2139.
32. Rogaski, B., and J. B. Klauda. 2012. Membrane-binding mechanism of a peripheral membrane protein through microsecond molecular dynamics simulations. *Journal of molecular biology*. 423(5):847-861.
33. Jo, S., T. Kim, V. G. Iyer, and W. Im. 2008. CHARMM-GUI: a web-based graphical user interface for CHARMM. *Journal of computational chemistry*. 29(11):1859-1865.
34. Jo, S., J. B. Lim, J. B. Klauda, and W. Im. 2009. CHARMM-GUI Membrane Builder for mixed bilayers and its application to yeast membranes. *Biophysical journal*. 97(1):50-58.
35. Qi, Y., X. Cheng, J. Lee, J. V. Vermaas, T. V. Pogorelov, E. Tajkhorshid, S. Park, J. B. Klauda, and W. Im. 2015. CHARMM-GUI HMMM builder for membrane simulations with the highly mobile membrane-mimetic model. *Biophysical journal*. 109(10):2012-2022.
36. Wu, E. L., X. Cheng, S. Jo, H. Rui, K. C. Song, E. M. Dávila-Contreras, Y. Qi, J. Lee, V. Monje-Galvan, and R. M. Venable (2014). CHARMM-GUI membrane builder toward realistic biological membrane simulations. Wiley Online Library.
37. Wildermuth, K. D., V. Monje-Galvan, L. M. Warburton, and J. B. Klauda. 2019. Effect of membrane lipid packing on stable binding of the ALPS peptide. *Journal of chemical theory and computation*. 15(2):1418-1429.

38. Jo, S., T. Kim, and W. Im. 2007. Automated builder and database of Protein/Membrane complexes for molecular dynamics simulations. *PLoS One*. 2(9):e880.
39. Jorgensen, W. L., J. Chandrasekhar, J. D. Madura, R. W. Impey, and M. L. Klein. 1983. Comparison of simple potential functions for simulating liquid water. *The Journal of chemical physics*. 79(2):926-935.
40. Li, Z., R. M. Venable, L. A. Rogers, D. Murray, and R. W. Pastor. 2009. Molecular dynamics simulations of PIP2 and PIP3 in lipid bilayers: determination of ring orientation, and the effects of surface roughness on a Poisson-Boltzmann description. *Biophysical journal*. 97(1):155-163.
41. Lee, J., X. Cheng, J. M. Swails, M. S. Yeom, P. K. Eastman, J. A. Lemkul, S. Wei, J. Buckner, J. C. Jeong, and Y. Qi. 2016. CHARMM-GUI input generator for NAMD, GROMACS, AMBER, OpenMM, and CHARMM/OpenMM simulations using the CHARMM36 additive force field. *Journal of chemical theory and computation*. 12(1):405-413.
42. Brooks, B. R., C. L. Brooks III, A. D. Mackerell Jr, L. Nilsson, R. J. Petrella, B. Roux, Y. Won, G. Archontis, C. Bartels, and S. Boresch. 2009. CHARMM: the biomolecular simulation program. *Journal of computational chemistry*. 30(10):1545-1614.
43. Phillips, J. C., R. Braun, W. Wang, J. Gumbart, E. Tajkhorshid, E. Villa, C. Chipot, R. D. Skeel, L. Kale, and K. Schulten. 2005. Scalable molecular dynamics with NAMD. *Journal of computational chemistry*. 26(16):1781-1802.
44. Phillips, J. C., D. J. Hardy, J. D. Maia, J. E. Stone, J. V. Ribeiro, R. C. Bernardi, R. Buch, G. Fiorin, J. Hénin, and W. Jiang. 2020. Scalable molecular dynamics on CPU and GPU architectures with NAMD. *The Journal of chemical physics*. 153(4):044130.
45. Ryckaert, J.-P., G. Ciccotti, and H. J. Berendsen. 1977. Numerical integration of the cartesian equations of motion of a system with constraints: molecular dynamics of n-alkanes. *Journal of computational physics*. 23(3):327-341.
46. Hoover, W. G. 1985. Canonical dynamics: Equilibrium phase-space distributions. *Physical review A*. 31(3):1695.
47. Feller, S. E., Y. Zhang, R. W. Pastor, and B. R. Brooks. 1995. Constant pressure molecular dynamics simulation: the Langevin piston method. *The Journal of chemical physics*. 103(11):4613-4621.
48. Martyna, G. J., D. J. Tobias, and M. L. Klein. 1994. Constant pressure molecular dynamics algorithms. *The Journal of chemical physics*. 101(5):4177-4189.
49. Steinbach, P. J., and B. R. Brooks. 1994. New spherical-cutoff methods for long-range forces in macromolecular simulation. *Journal of computational chemistry*. 15(7):667-683.
50. Darden, T., D. York, and L. Pedersen. 1993. Particle mesh Ewald: An N· log (N) method for Ewald sums in large systems. *The Journal of chemical physics*. 98(12):10089-10092.
51. Humphrey, W., A. Dalke, and K. Schulten. 1996. VMD: Visual molecular dynamics. *Journal of Molecular Graphics*. 14(1):33-38, http://www.sciencedirect.com/science/article/B6VNC-3VJRDJX-5/2/247595492d1cae80b34bed4d649bf0b2.
52. Drin, G., J.-F. Casella, R. Gautier, T. Boehmer, T. U. Schwartz, and B. Antonny. 2007. A general amphipathic α-helical motif for sensing membrane curvature. *Nature structural & molecular biology*. 14(2):138-146.

53. Monje-Galvan, V., and J. B. Klauda. 2018. Preferred binding mechanism of Osh4's amphipathic lipid-packing sensor motif, insights from molecular dynamics. *The Journal of Physical Chemistry B*. 122(42):9713-9723.